academicJournals

Vol. 8(21), pp. 902-916, 4 June, 2013
DOI 10.5897/SRE12.513
ISSN 1992-2248 © 2013 Academic Journals
http://www.academicjournals.org/SRE

Scientific Research and Essays

Full Length Research Paper

Experimental and numerical stress analysis of glass fiber-reinforced polymer (GFRP) -stiffened shells with cutout under axial loading

Saleh Yazdani and GH Rahimi*

Department of Mechanical Engineering, Tarbiat Modares University, P. O. Box: 14115-143 Tehran, Iran.

Accepted 14 May, 2013

In the present study, the stress analysis of thin-walled glass fiber-reinforced polymer (GFRP) cylindrical shells with and without cutout subjected to axial loading was carried out by using experimental and finite-element method. The effect of cutout type on the stress distribution of the shell was described. In the experimental procedure electrical strain gauges were used to measure the experimental strain at specific point of the structure. Finite-element analysis was included in a static analysis that predicts stress distribution and a buckling analysis that predicts the local buckling response of the models. The results illustrated that the stress concentration factor was completely related to cutout position on grid-stiffened shells. In particular, a local buckling response occurred in the shell near the cutout edge where the maximum stress gradient was reported. In addition, it has been concluded that stiffeners have good influence on reducing the stress concentration and changing the direction of the destructive loads on the shell.

Key words: Stress analysis, cutout, stiffened shells, composite shells, stress concentration factor (SCF).

INTRODUCTION

Grid-stiffened composite structures due to high strength and stiffness and their light weight have been widely used in the aircraft industry. One of these structures is grid-stiffened composite cylindrical shells that are widely used in the fuselage of aircrafts and in the body of missiles. Grid-stiffened shells are cylinders with stiffeners either on the inner, outer or both sides of the shell. Using stiffeners increases the load resistance in the shell without too much increasing in the weight. To reduce the weight of these structures polymer fibers were used to manufacture the shell and the stiffeners. Moreover, to reduce the cost of the construction of the grid-stiffened cylinders, new production method, filament winding, in which the fibers automatically lie in special places, have been used (Wodesenbet et al., 2003). These structures due to their ribs have good reliability and efficiency. The specific buckling load of these shells is very high. Therefore, mostly, buckling analysis of these structures has been investigated (Vasiliev et al., 2001; Buragohain and Velmurugan 2011; Kidane et al., 2003). There are a few published researches in the literature in the field of stress analysis of grid-stiffened composite cylindrical shells with or even without cutout. Yazdani et al. (2009) studied the buckling behavior of glass fiber-reinforced polymer (GFRP) unstiffened and stiffened cylindrical shells. Their specimens consisted of unstiffened shells and stiffened shells with hexagonal, triangular, and lozenge grids fabricated by filament winding process. All the specimens

*Corresponding author. E-mail: rahimi_gh@modares.ac.ir. Tel: (+98) 218288-3356. Fax: (+98) 8288-4909.

subjected to axial loading and general failure and local failure modes of them were observed. The effects of the number of helical ribs and grid shapes into the buckling behavior of stiffened shells have been investigated by Yazdani and Rahimi (2010), too. They concluded that the lozenge grid with adequate helical ribs is the best choice for axial compression loading. This conclusion is the basis of choosing lozenge grid in the present work. Yazdani and Rahimi (2011) investigated the behavior of GFRP-stiffened and –unstiffened shells under cyclic axial loading and unloading. They observed that for cyclic loading, using stiffened shells is better than using unstiffened shells. Moreover, the effect of stiffener profile on buckling strength in composite isogrid stiffened shell under axial loading has been investigated (Rahimi et al., 2011).

Morozov et al. (2011) investigated the buckling behavior of cylindrical composite lattice shells under axial compression, transverse bending, pure bending, and twisting loading. They also investigated the effect of the cutout on the buckling load of the structures. They concluded that the buckling load completely depends on the size of the cutout.

Many researchers have studied on cutout problems to predict the stress distribution around the cutout in both plates and shells while a few works are available on the grid-stiffened shells with cutout. Han et al. (2006) investigated the response of aluminum cylinder with a cutout subject to axial compression. Ryu et al. (2004) studied the stress analysis of the orthotropic composite cylindrical shell with circular and elliptical cutout. They used strain gauges in their experimental tests in order to obtain the stress concentration factor; therefore, in the present work this method was used. Stress distribution on the grid-stiffened composite cylindrical shell with circular cutout under axial compression investigated by Yazdani and Rahimi (2011).

Stress concentration around the cutouts is important in the practical engineering. The ultimate tensile strength of the specimens with cutout or notch was reduced. For instance, the strength reductions of 40 to 60% have been reported for a glass fiber reinforced plastic plate due to the existence of cutout (Adam, 1986). Stress distribution of an infinite orthotropic composite laminate with an elliptical cutout developed by Lekhnistskii et al. (1968). Figure 1 shows the schematic view of the laminate with its coordinate system at the center of it.

By assuming an elliptical cutout with major and minor radius *a* and *b*, Stress Concentration Factor (SCF) around the cutout can be achieved as:

$$K_T^{\infty} = 1 + \frac{a}{b}\sqrt{2\left(\sqrt{\frac{E_y}{E_x}} - v_{yx}\right) + \frac{E_y}{G_{xy}}} \quad (1)$$

Table 1. Nominal material properties.

Material properties	Symbols	E-glass/Epoxy
Longitudinal modulus	E_L	32 GPa
Transverse modulus	E_T	4.8 GPa
Shear modulus	G_{LT}	3.1 GPa
Poisson's ratio	v_{LT}	0.3

where K_T^{∞} is stress concentration factor; E_x, E_y and G_{xy} are the laminate extensional and shear moduli, respectively; v_{xy} denotes the effective laminate Poisson's ratio. In Equation (1), by considering *a*=*b*, the SCF for orthotropic laminate with circular cutout can be obtained as:

$$K_T^{\infty} = 1 + \sqrt{2\left(\sqrt{\frac{E_y}{E_x}} - v_{yx}\right) + \frac{E_y}{G_{xy}}} \quad (2)$$

In this paper, the stress analysis for the grid-stiffened composite shells with four types of cutout subjected to an axial compression load was carried out using experimental and finite element methods. Moreover, stress analysis of the shell without cutout was investigated. The various cutout types were defined to compare the effect of these on the stress distributions. Experimental stress analyses were obtained in the elastic region using the strain gauges which were attached on the outer surface of the shells. Strain gauges were attached in a path which was started at the cutout edge and it was continued toward the ribs' intersections (path-1) and to the upper edge of the shell (path-2). In addition, the Finite-Element (FE) analysis was performed by using ABAQUS 6.10 commercial software.

EXPERIMENTAL PROCEDURE

Specimen preparation

The specimens were consisted of a shell and six reinforcement helical ribs, three clockwise and three counter clockwise, which were fabricated using special filament winding machine. Moreover, two special epoxy rings were used at both ends of the shells to obtain simply support boundary condition and avoid local boundary damages at the edges. E-glass fiber and epoxy type cy219 were used in manufacturing and the specimens were produced in room temperature. Shell winding angle was ±76°. Nominal material properties are given in Table 1.

The machine first lays the fibers in the helical grooves to make the stiffeners and then wraps continues fiber around the cylindrical mandrel to make the skin. The details of the manufacturing procedure are available in the former works (Yazdani et al., 2009;

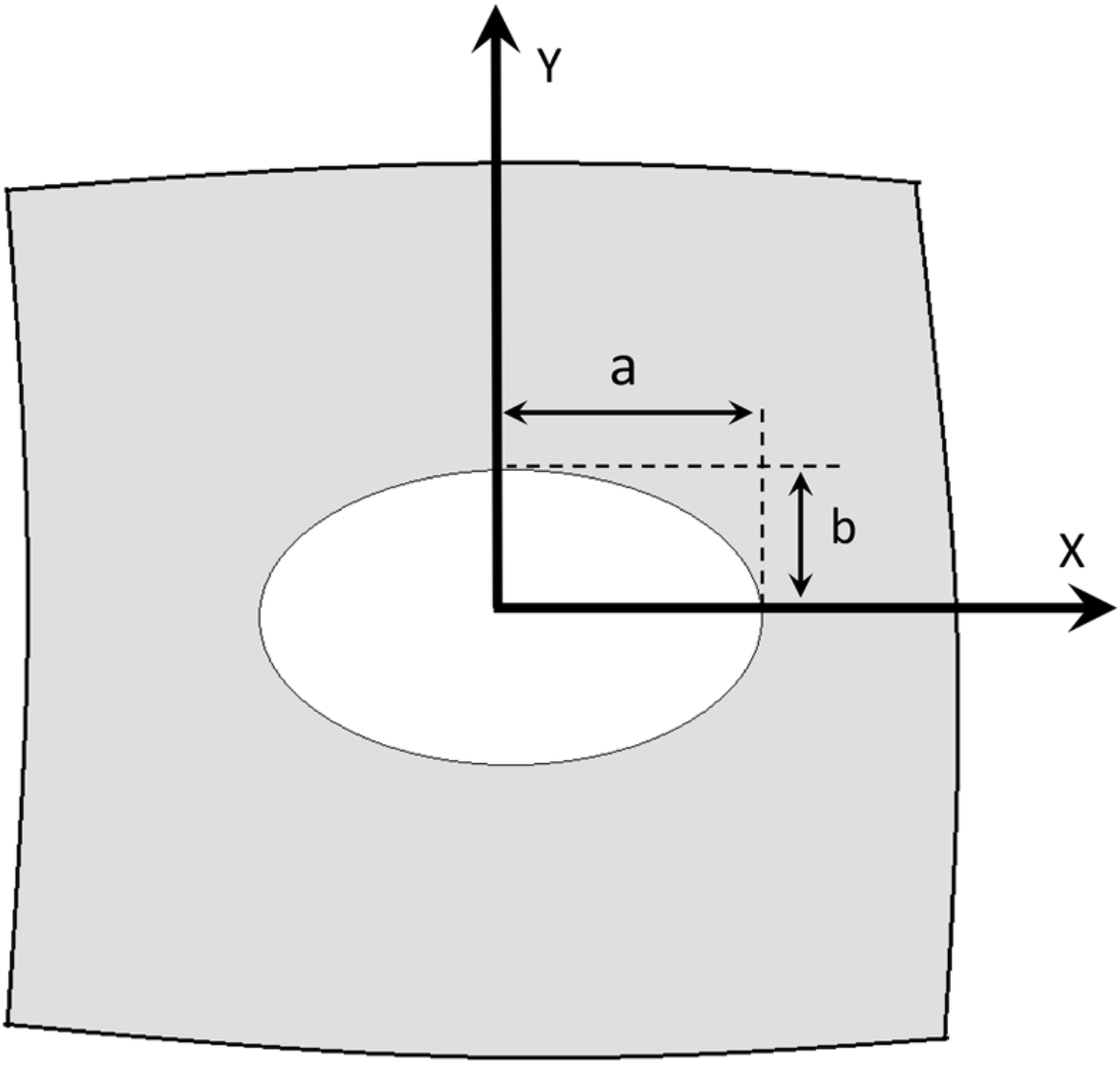

Figure 1. Schematic view of the laminate with elliptical cutout.

Yazdani and Rahimi, 2010, 2011). Figure 2 shows the filament winding machine.

Five specimens (one without cutout and four with circular, square, and elliptical cutout types) were fabricated. Figure 3 shows the specimens.

All the specimens had the same conditions in production and the same sizes. In all the specimens, cutout was created in the same position which was of 102 mm of the upper edge of the shells. The diameter of the circular cutout was d=10 mm, for the elliptical cutouts in one case the major diameter d_1 was aligned to the load direction (elliptical cutout 1) and in the other one the minor diameter d_2 was aligned to the load direction (elliptical cutout 2). Diameters in elliptical cutouts were d_1=20 mm and d_2=10 mm and for the specimen with square cutout the length of the cutout was a=10 mm. For obtaining strain gradient, strain gauge method was used. Strain gauges were attached on the outer surface of the shells in two directions at each point, while strain gauge rosette was used for area near the cutout because of high amount of shear strains. Moreover, two strain gauges were attached on the same distance from the shell's edge at the other side of it for measuring the stresses at infinite and were used for calculating the stress concentration factor equation. The position of strain gauges on the shell's surface is shown in Figure 4.

Test procedure

The test components were tested in INSTRON 5500R universal machine under axial compression with cross-head speed of 1.3 mm/min which provides static loading conditions based on the ASTM D6641 standard. Strain values in each step of loading were recorded by DATA logger device. Figure 5 shows the test setup of the specimen.

The strain values of all the specimens were recorded exactly at

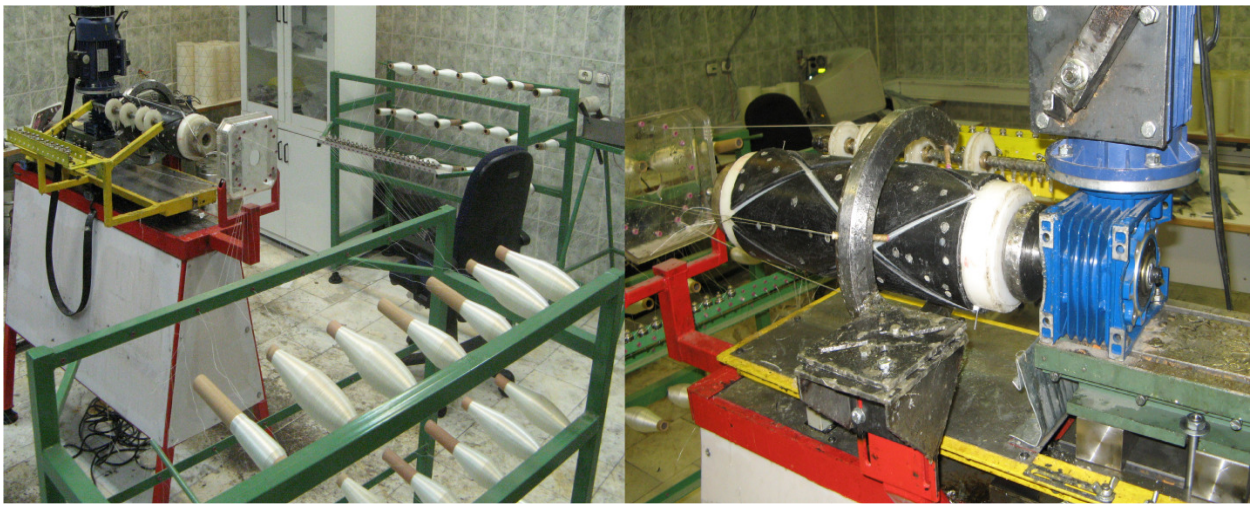

Figure 2. Filament winding machine.

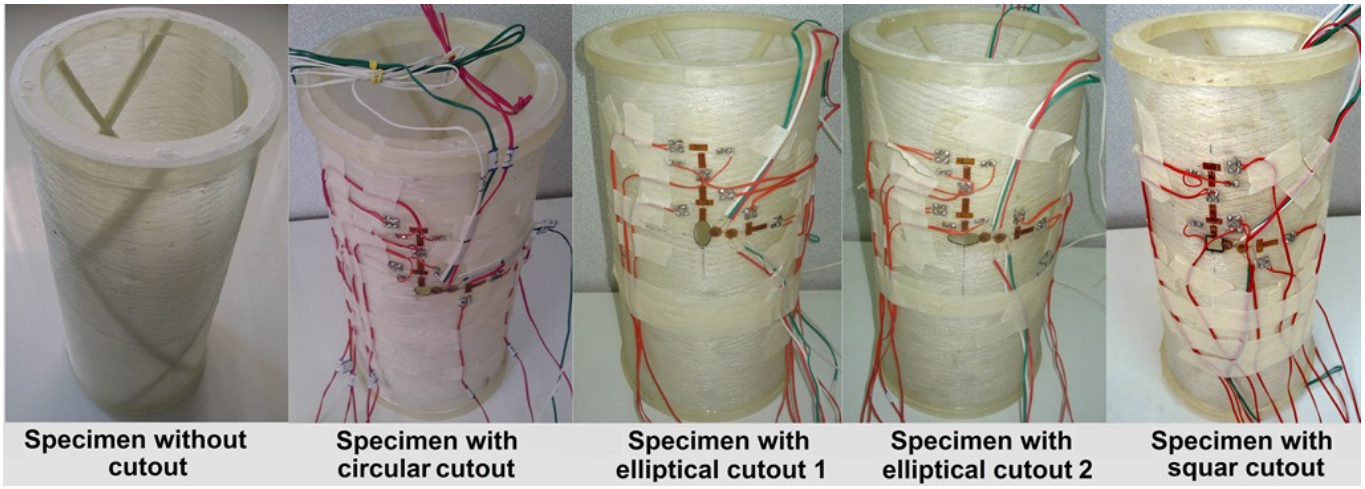

Figure 3. Specimens used in the experimental work.

loading 3 KN and were used to obtain stress distribution by using stress-strain relations in composite materials. Equation (3) to (6) was used to obtain stress distributions through amount of strains.

$$\begin{bmatrix}\sigma_x\\ \sigma_y\\ \tau_{xy}\end{bmatrix}=\left[\overline{Q}\right]\begin{bmatrix}\varepsilon_x\\ \varepsilon_y\\ \gamma_{xy}\end{bmatrix} \quad (3)$$

$$\left[\overline{Q}\right]=\left[T\right]^{-1}\left[Q\right]\left[T\right]^{-T} \quad (4)$$

$$\left[T\right]=\begin{bmatrix}\cos^2\theta & \sin^2\theta & 2\sin\theta\cos\theta\\ \sin^2\theta & \cos^2\theta & -2\sin\theta\cos\theta\\ -\sin\theta\cos\theta & \sin\theta\cos\theta & \cos^2\theta-\sin^2\theta\end{bmatrix} \quad (5)$$

$$Q_{11}=\frac{E_1}{1-v_{12}v_{21}},\ Q_{22}=\frac{E_2}{1-v_{12}v_{21}},\ Q_{12}=\frac{v_{12}E_2}{1-v_{12}v_{21}},\ Q_{66}=G_{12} \quad (6)$$

[Q] represents the transformed reduced matrix; E_1 and E_2 are Young's modulus; v_{12} and v_{21} are Poisson's ratio, and θ is the angle from the principal axis to x-y axis. Halpin-Tsai equation-developed by Ashton et al. (1969) - were used to determine mechanical properties of the component, separately.

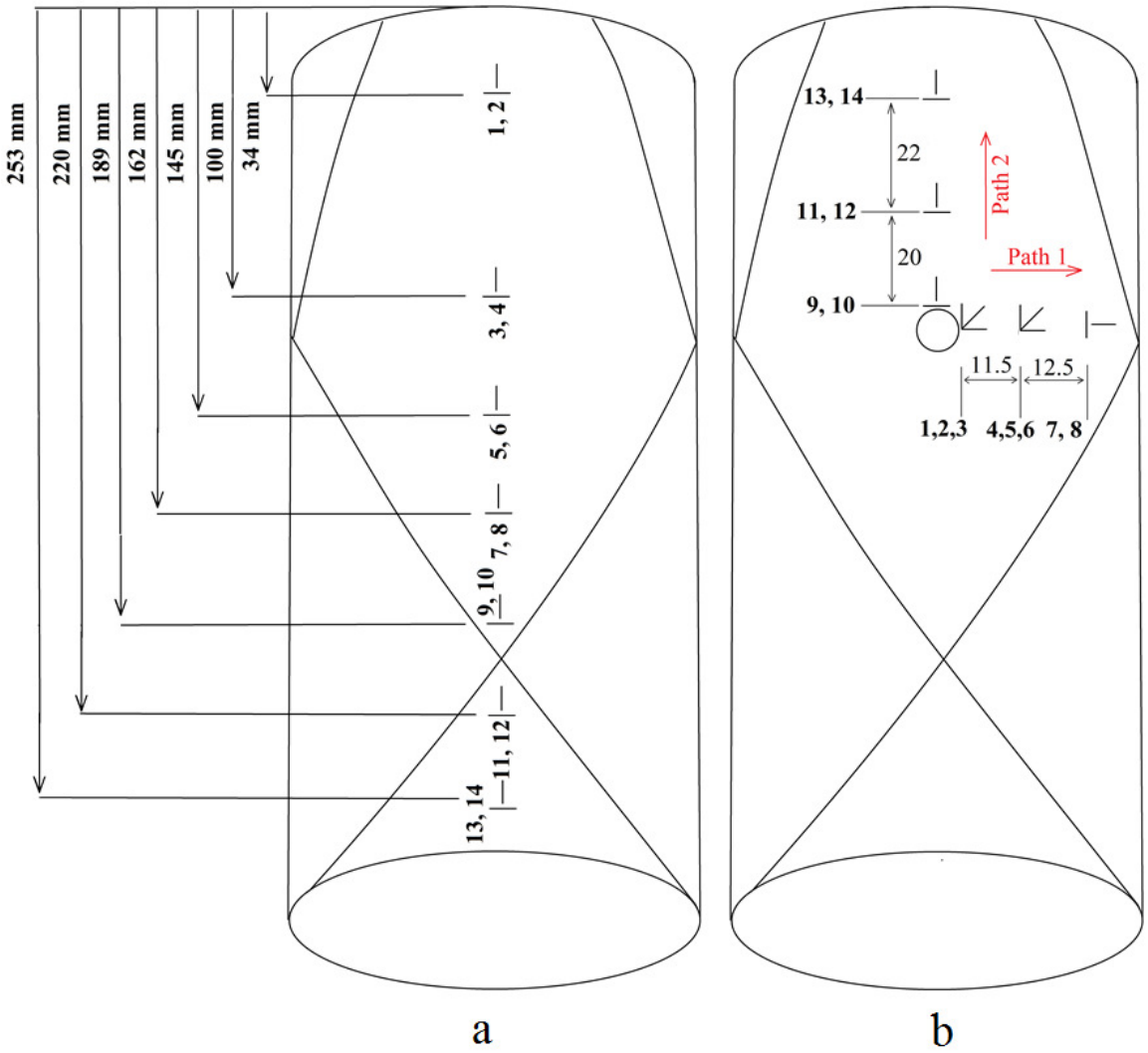

Figure 4. Position of strain gauges: a) stiffened shell without cutout; b) stiffened shell with cutout.

Table 2. Geometrical dimensions of the models.

Shell (mm)		Stiffener	
Height	275	Cross-section area	6×6 mm
Outer diameter	140	Orientation	30°
Thickness	1		

Finite element analysis

Numerical simulations have been performed using general purpose for finite element program ABAQUS 6.10 standard. There was no symmetry in the geometry and material properties in the model. Therefore, it has been modeled completely. The numerical models had the same dimensions of the experimental specimen for the comparison and are reported in Table 2.

Mesh, loading, and boundary conditions

The shell was meshed by an eight nodes reduced integration shell elements (S8R) which is based on a Reissner-Mindlin element. For the stiffener, advanced 3D stress quadrilateral element (C3D20R) was used. All the parts were partitioned to lay the nodes of the shell and ribs at the shell-stiffeners interfaces. Stiffeners and the shell were constrained at the interfaces using shell to solid coupling in ABAQUS. To apply pure axial compression, using the coupling technique in the software, all the nodes on each end cross-section were kept on the same respective plane and were constrained to one reference point to satisfy the classic laminated theory conditions. All the boundary conditions and loading were applied at the reference point (RP), which exactly models the experimental conditions. Several different FE models with different levels of mesh refinement and different types of constraint for interface of the stiffeners and the shell have been developed. In addition, arrangement and type of element schemes have been changed

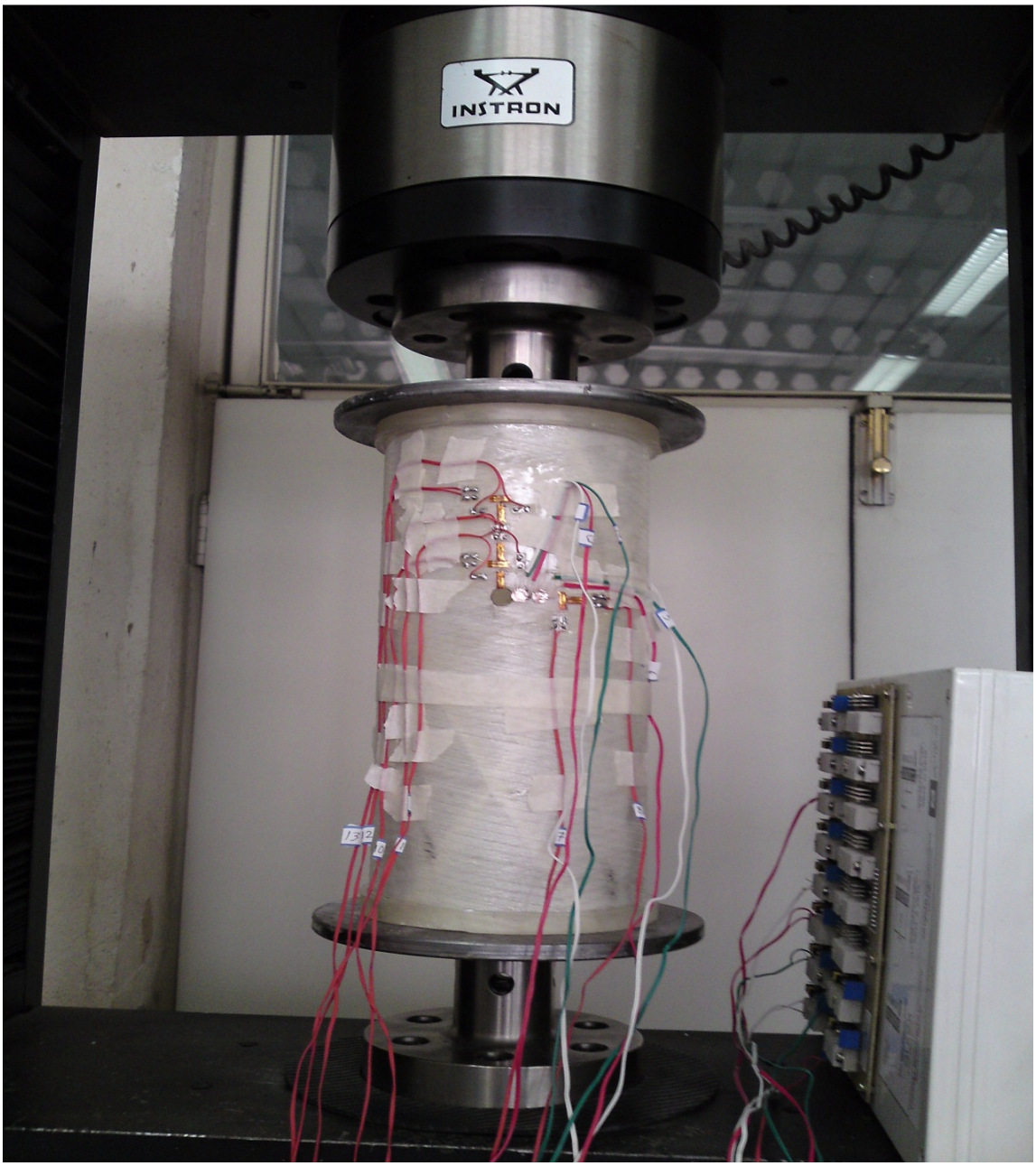

Figure 5. Experimental testing setup.

several times to achieve converged results, and then accurate results were selected. Figure 6 shows the FE mesh and constraints.

Analysis

In the current study, the general/static method has been employed. All the models were subjected to compression load F=3 KN. In addition, first buckling mode of the stiffened shell was obtained under the applied load for comparing with experimental deformed shape of the specimens. Figure 7 shows the Von-Mises stress distribution in models after subjecting to the compression loading.

RESULTS AND DISCUSSION

All the results are classified into specimens without cutout and specimen with cutout. Stress distributions and stress concentration factor (SCF) were obtained by the two

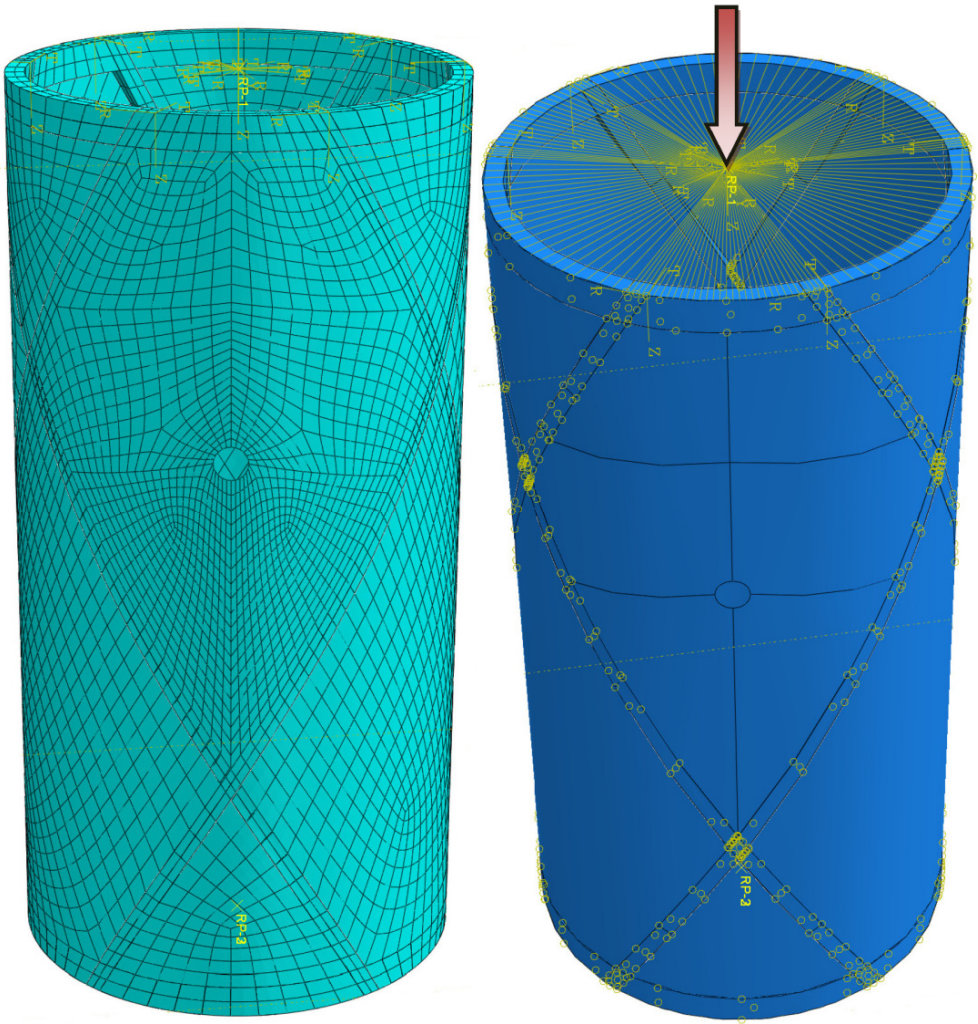

Figure 6. FE meshed model and constraints.

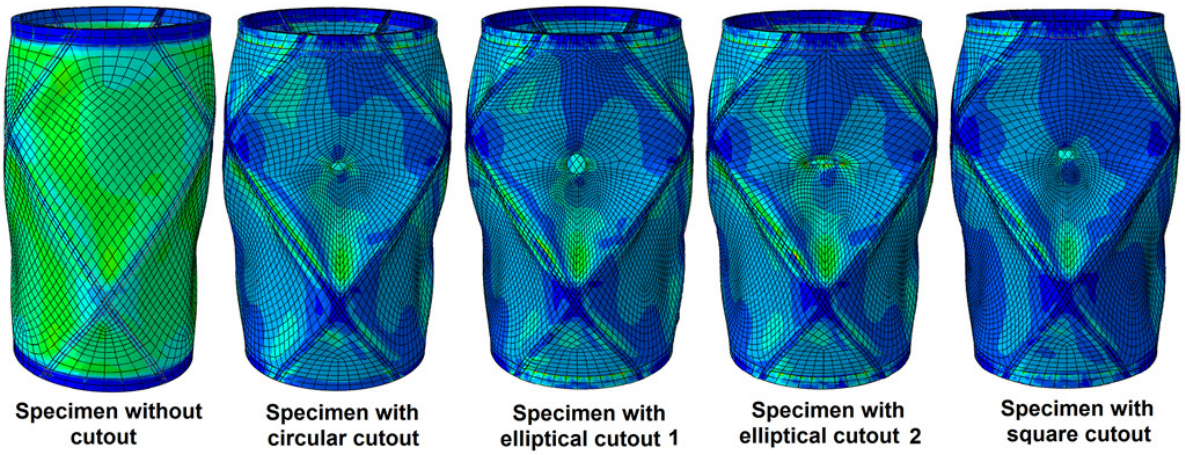

Figure 7. Von-Mises stress distribution in the grid-stiffened shells.

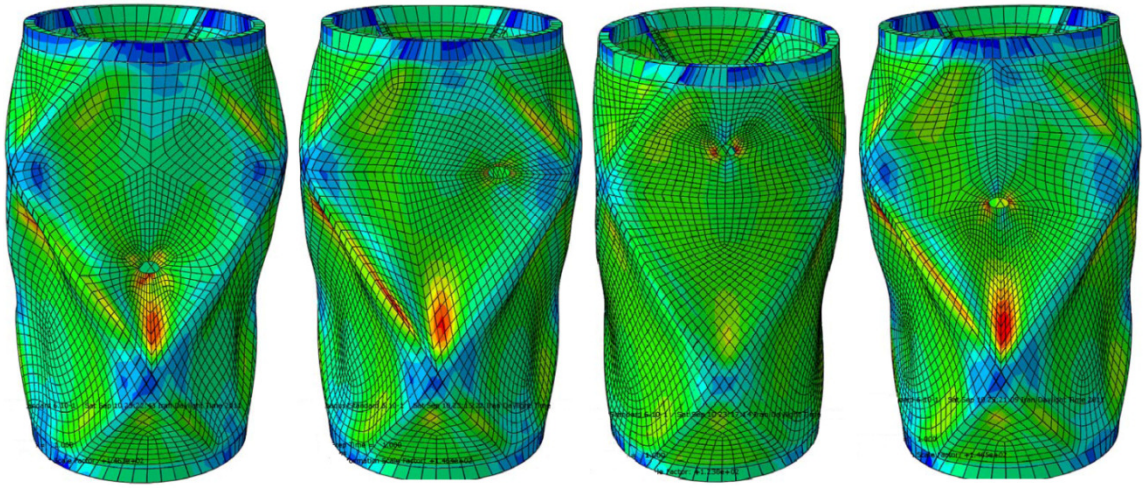

Figure 8. Von-Mises stress distribution of stiffened shells with cutout.

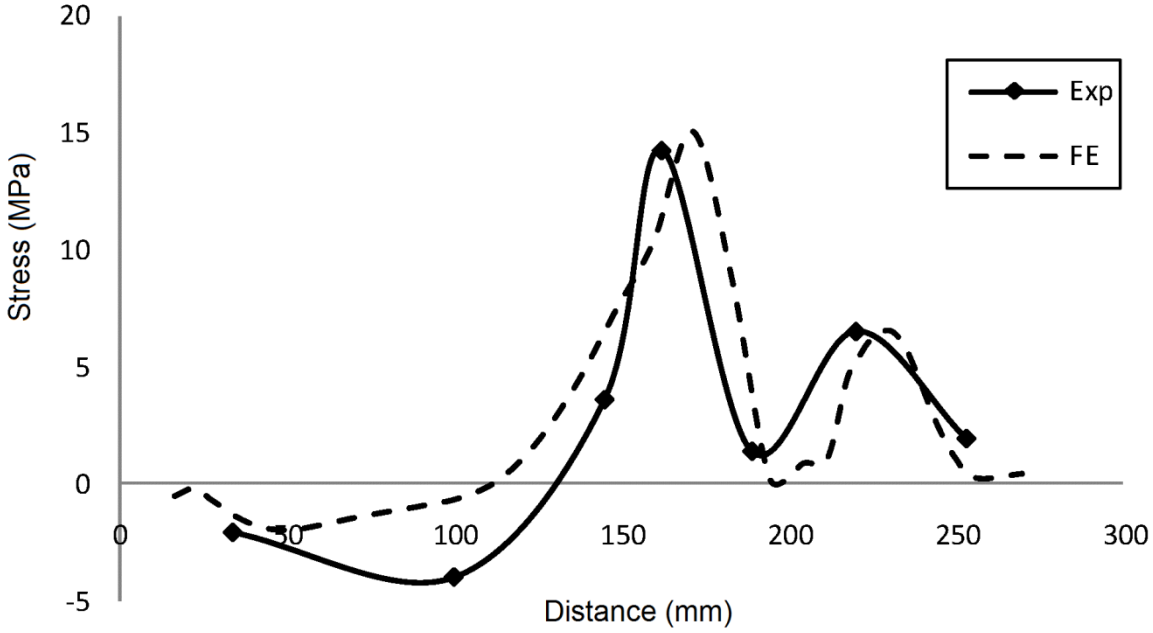

Figure 9. Axial stress distribution on the specimen without cutout.

methods. Before creating cutout in the specimens, initial FE models with circular cutout were developed to investigate the maximum stress value at $\theta=\pi/2$ according to the other researcher's conclusion (Ryu et al., 2004). It was observed that stress concentration exactly depends on the position of the cutout on the shell. Therefore, several different models were developed and the position of cutout has been changed until the maximum stress distribution appeared at $\theta=\pi/2$. Final position was used in the experiment. Cutouts were created in the middle of the models, near the intersection of the ribs, and near the upper edge. Figure 8 shows the attempts for modeling the shells with cutouts.

The differences among the stress distribution of stiffened shells with cutout demonstrate the effect of the stiffener in changing the load direction on the shell. Figures 9 and 10 show the stress distribution of the specimen without cutout in axial and hoop directions,

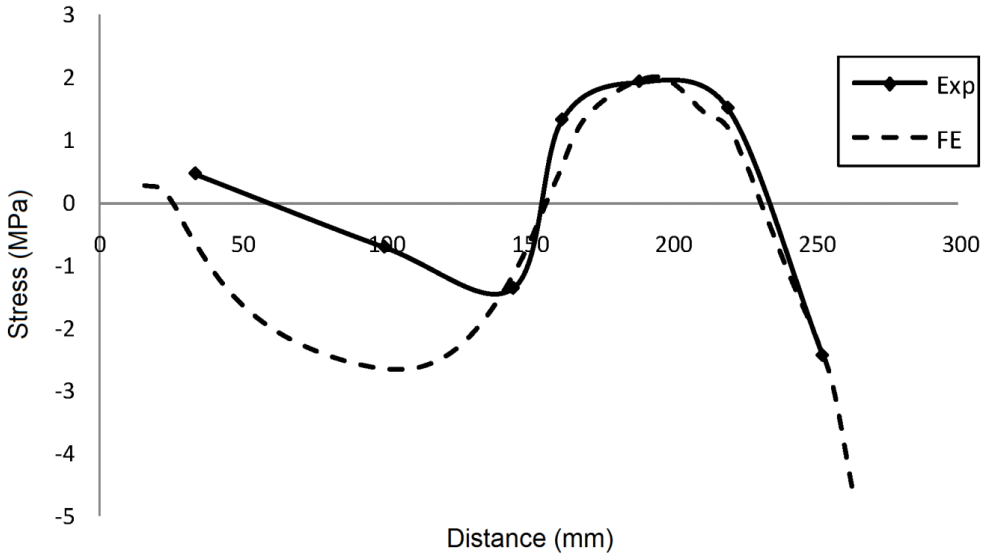

Figure 10. Hoop stress distribution on the specimen without cutout.

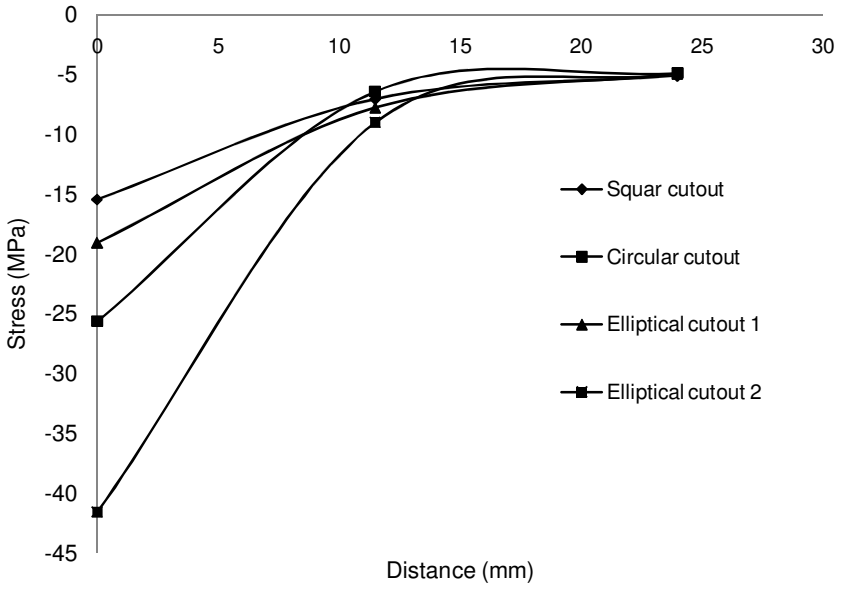

Figure 11. Axial stress in path-1.

respectively.

Stress distributions in hoop and axial directions have different values through the top end to the bottom end of the shell. Maximum values of stress were belonged to strain gauges 7 and 8, but this amount of stress was reduced suddenly by reaching to the ribs' intersection on the shell. It means that stiffeners have good influence on reducing the stress intensity. Minimum stress values were reported for the strain gauges 9 and 10.

According to the type of loading, negative values of axial stress were expected, but stress values close the ribs' intersection had positive values. It shows the ribs' effect in changing the destructive load direction. This effect can be observed in hoop stresses, too.

The distribution of axial stress in path-1 for specimens with cutout is shown in Figure 11. The maximum axial stress was occurred in specimen with elliptical cutout 2, especially close to its cutout edge. According to the

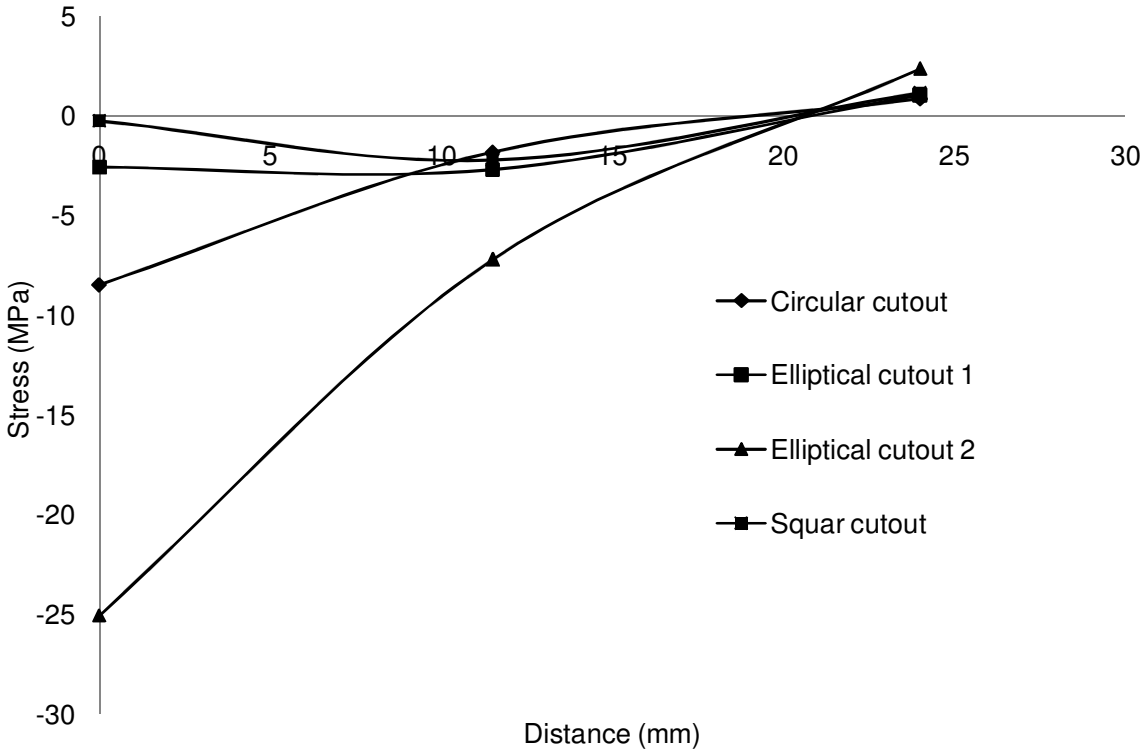

Figure 12. Hoop stress in path-1.

Table 3. Stress values for the reference point.

Axial stress	Hoop stress	Shear stress
-6.8588 Mpa	0.718 Mpa	-1.17 Mpa

Figure 11, the axial stress at the point away from the cutout was reduced. It can be attributed to the stiffeners effect in causing the shell to be stiff, which is significant. In specimen with square cutout, the minimum axial stress was occurred. In all the specimens, axial stress was negative and maximum values in path-1 were reported at the cutout edge.

The distribution of hoop stress in path-1 is shown in Figure 12. According to this figure, the maximum hoop stress near the cutout edge was happened in the specimen with elliptical cutout 2, which was five times greater than the one of the specimen with elliptical cutout 1 and square cutout. It can be related to the greater values of shear stress, which was recorded. In the stress distribution in path-1, the specimen with square cutout was demonstrated the best performance and the specimen with elliptical cutout 2 had the worst performance. It causes to appear the first mode of buckling in this type of cutout faster than the other ones, which was observed specifically in buckling analysis.

The distribution of axial stress in path-2 is shown in Figure 13. The axial stress distribution had more values at points away from the cutout edge in path-2 direction. Maximum stress values have been recorded for the specimen with elliptical cutout 1 in this path. Therefore, stress distribution in the specimen with elliptical cutout was depended on the loading direction and the major diameter direction as well.

The distribution of hoop stress in path-2 is shown in Figure 14. There was no significant difference between the specimens except the specimen with elliptical cutout 2. The stress values close to the cutout's edge had greatest values and were decreased by getting away from the cutout edge.

In all the specimens, by getting away from the cutout edge, stress distributions were tended to the close results. It means that the effect of the cutout is only related to the local damages. The stress values in path-1 had greater values than that the ones in path-2.

The stress values on the other side of the shell on the same place which contains no cutouts represent in Table 3 and were used as a reference point to find the stress concentration factors.

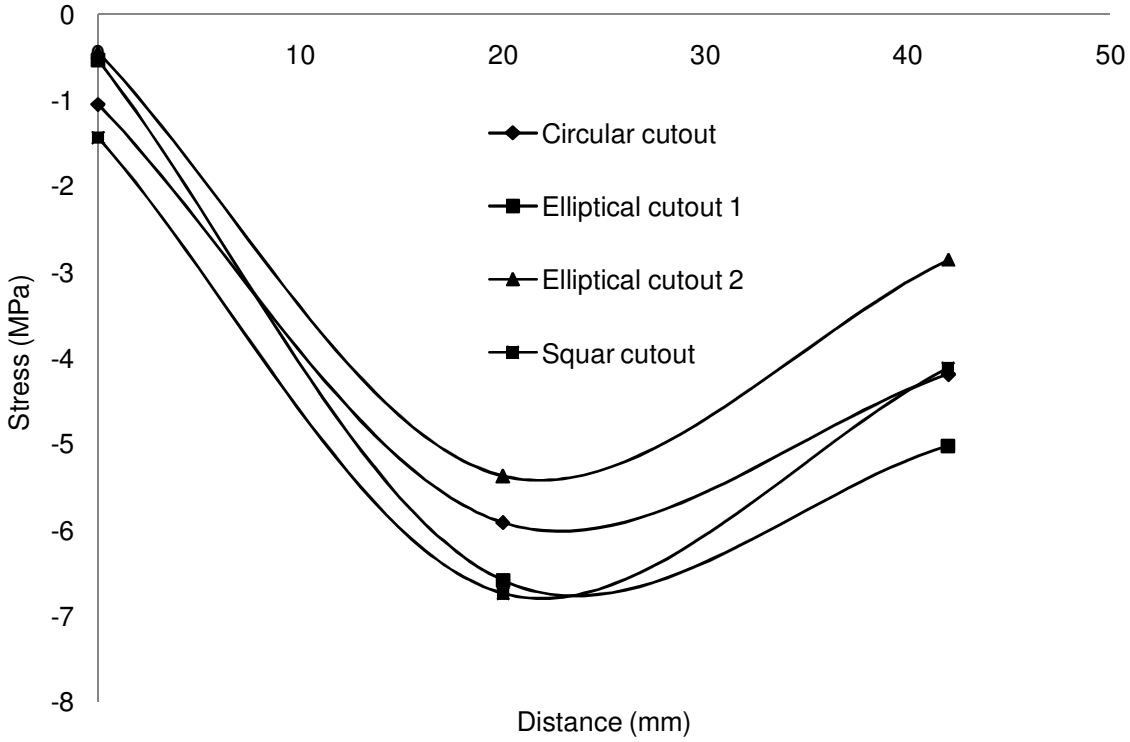

Figure 13. Axial stress in path-2.

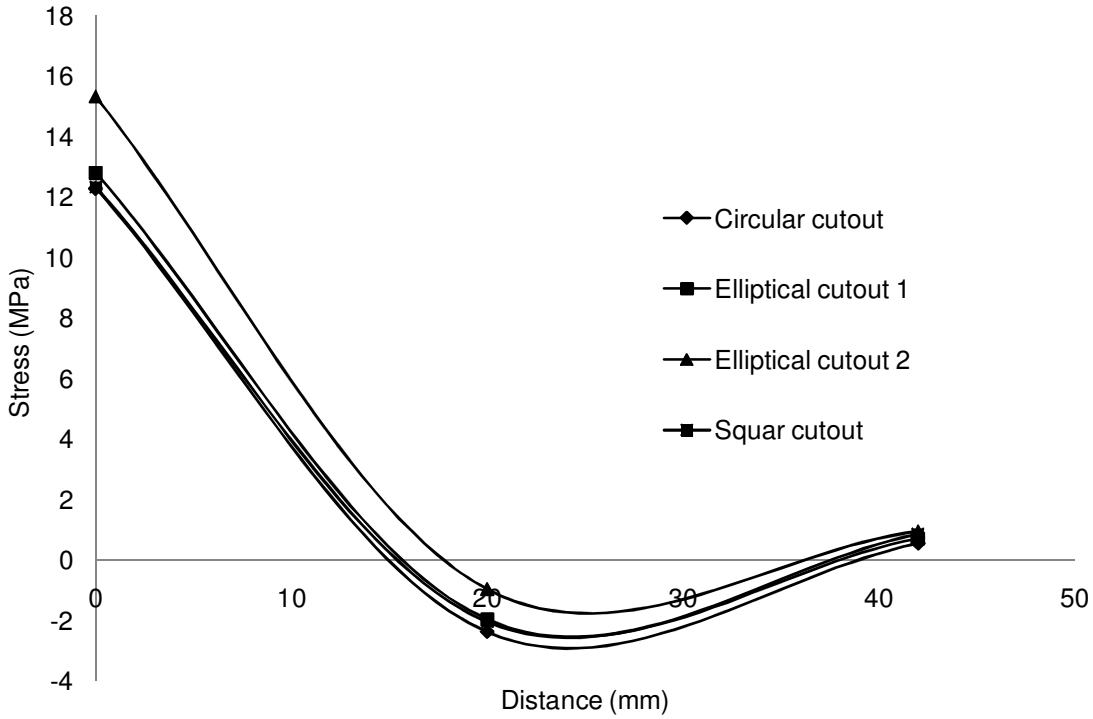

Figure 14. Hoop stress in path-2.

Table 4. SCF on the grid-stiffened composite cylindrical shell with cutout.

Type of specimen	Experimental SCF	FE SCF
Specimen with circular cutout	3.153	3.21
Specimen with elliptical cutout 1	2.87	2.9
Specimen with elliptical cutout 2	6.062	6.15
Specimen with square cutout	2.251	2.31

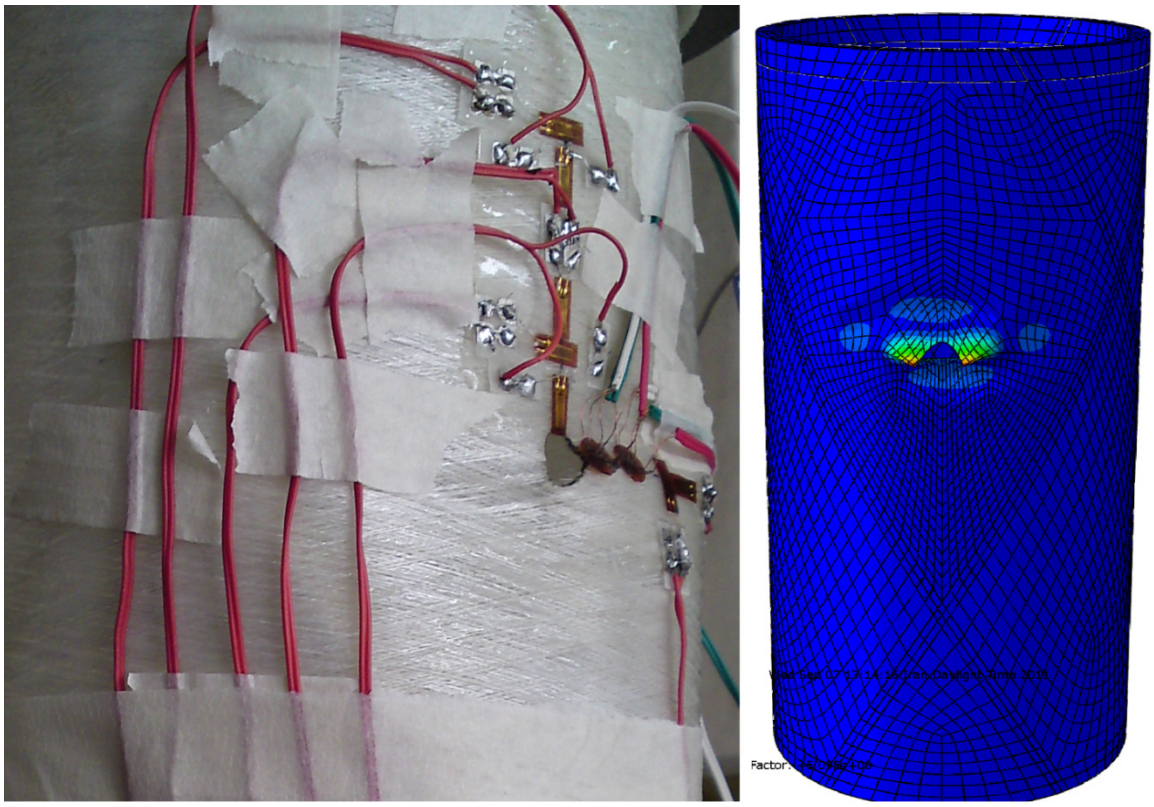

Figure 15. First buckling mode of the specimen with circular cutout.

Table 4 represents experimental and FE stress concentration factor (SCF) at $\theta=\pi/2$ on the grid-stiffened composite shells containing a cutout.

The values of SCF in experimental and FE analysis had close results. The maximum SCF value was related to the specimen with elliptical cutout 2 and minimum SCF was appeared in the specimen with square cutout. Therefore, for axial loading, by changing the elliptical cutout's major diameter opposite the load direction the SCF was dramatically increased.

To study the first buckling failure mode, different analyses were run by varying the cutout's type on the stiffened shell while maintaining the same configuration of stiffened shells. Figure 15 shows the first buckling mode of the specimen with circular cutout comparing with experimental results.

Figure 15 shows that the specimen fails in a local area. The buckling failure mode was appeared around the cutout, same as the experiment. Figure 16 shows the first buckling mode of the specimen with elliptical cutout 1 in comparison with the experiment.

Figure 16 shows that the buckling failure mode appears around the cutout, where the high stress values were reported. Figure 17 shows the first buckling shape of the specimen with elliptical cutout 2.

Figure 17 shows that the first buckling mode of the specimen with elliptical cutout 2 is related to the whole area around the cutout on the shell. However, in the

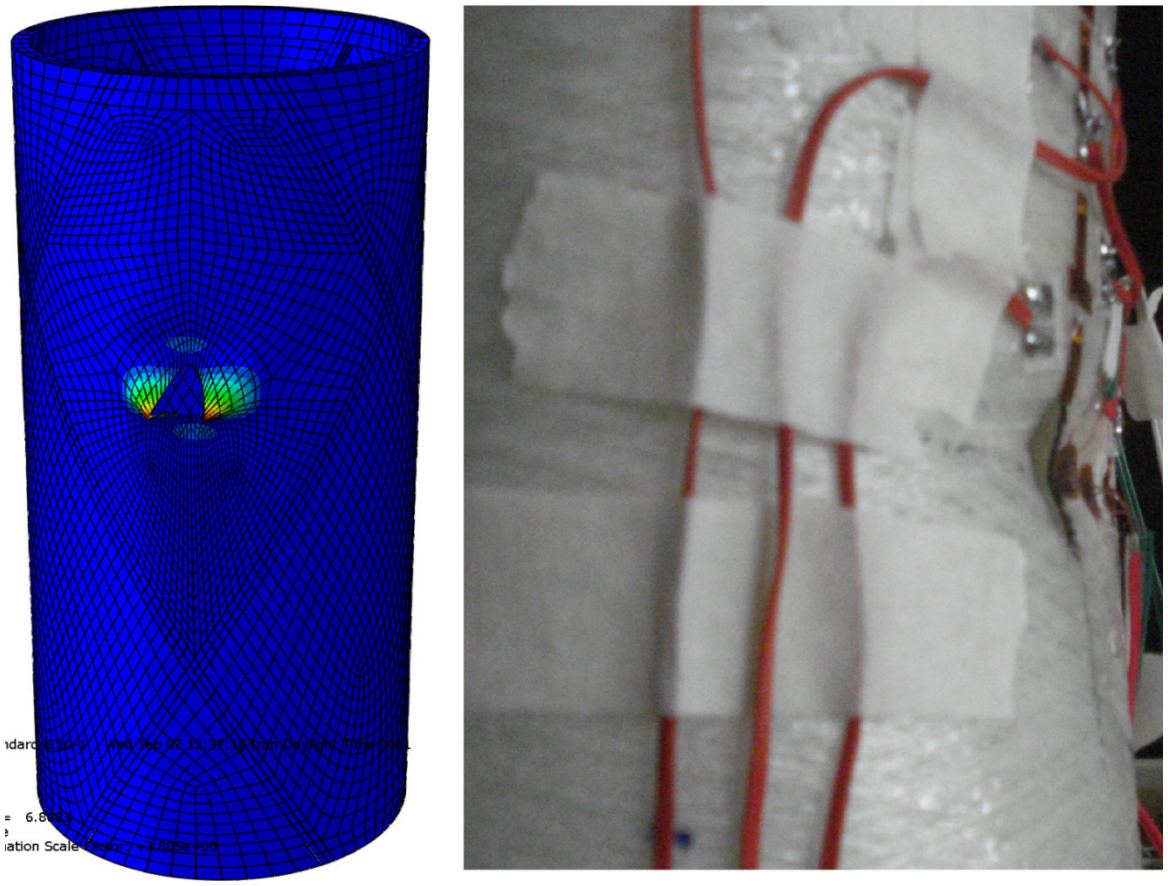

Figure 16. First buckling mode of the specimen with elliptical cutout 1.

experiment the deformed shape was related to the maximum stress area, same as the other specimens. Figure 18 shows the first buckling mode of the specimen with square cutout comparing with the experimental results.

The results show that the local buckling of the grid-stiffened cylindrical shell without any cutout under axial compression load appear on the whole shell, but, in grid-stiffened cylindrical shells with any type of cutout the local buckling was related to the cutout edge. The results also show that in all the specimens, FE results have been validated by the experimental results.

Conclusions

The stress analysis of grid-stiffened cylindrical shells with and without cutout under axial compression has been investigated using experimental and finite element modeling and analyses. The grid-stiffened shells with and without cutout have been manufactured by special filament winding machine. Four types of cutout were created on the shells in order to investigate the effect of cutout types on the stress concentration factor. By applying the strain gauge technique, strain distributions and consequently stress distributions have been obtained. Moreover, buckling analysis has been performed to investigate the local buckling behavior of the specimens in the two methods. In FE analysis, all the specimens were exhibited very close results to the experimental analysis. The following conclusions were achieved through this work:

1. In grid-stiffened cylindrical shells with each type of cutout, the location of maximum stress around the cutout was related to the cutout's position on the shell.
2. In both analyses, the buckling shape was in winding angle direction.
3. In the grid-stiffened shell with elliptical cutout, the direction of the major diameter had influence on the SCF and ultimate load of the specimen.
4. The maximum SCF belonged to the specimen with elliptical cutout 2 while the minimum SCF was exhibited by the specimen with square cutout.

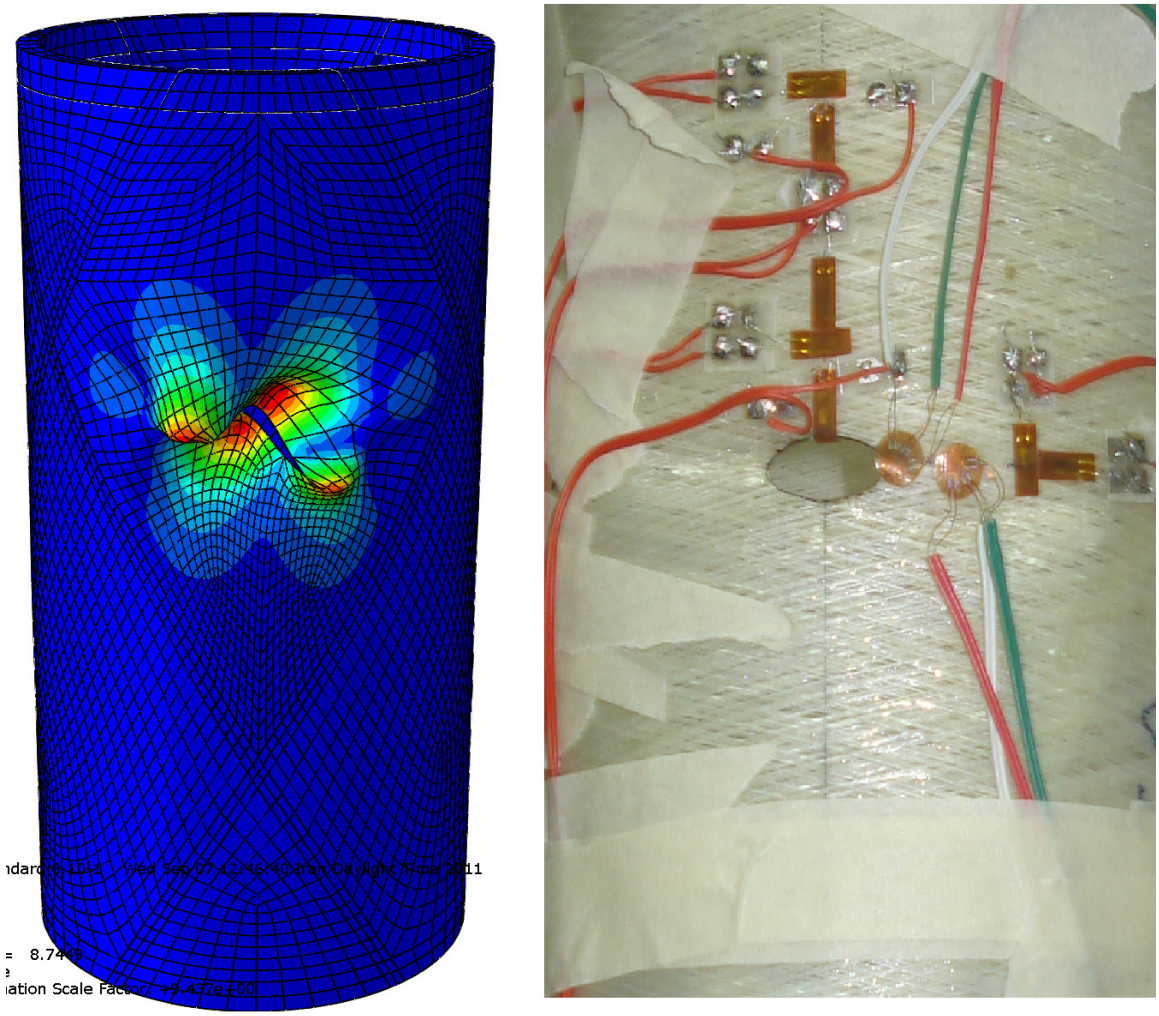

Figure 17. First buckling mode of the specimen with elliptical cutout 2.

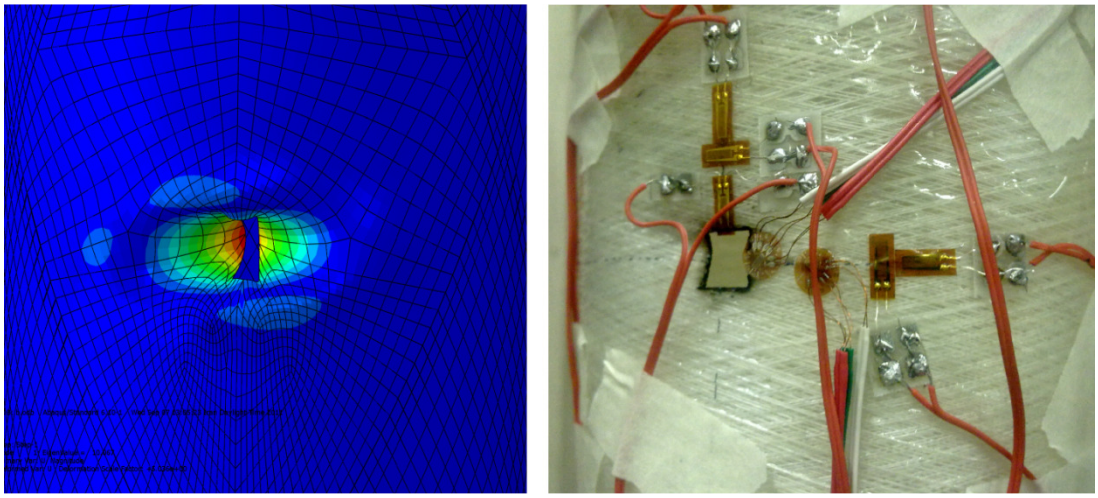

Figure 18. First buckling mode of the specimen with square cutout.

5. The stiffeners had good influence on reducing the stress values in all the specimens. Their influence was observed by testing the specimen without cutout.
6. Due to the stiffeners, stress values at the intersection of the ribs (on the shell) had positive values. This shows the effect of the stiffeners in changing the load direction and avoiding stress concentrations on the shell.
7. Stress values in the specimens with cutout at places near the stiffeners dramatically were decreased and were tended to the constant values.
8. In the experimental testing procedure, after unloading, the specimens back to its first shape because of using grid in their structure.

REFERENCES

Adam K (1986). The effect of cutouts on strength of GRP for naval ship hulls. Master Thesis, Department of Materials Science and Engineering, MIT, USA.
Ashton JE, Halpin JC, Petit PH (1969). Primer on Composite Materials. Technomic Press, Westport, CT.
Buragohain M, Velmurugan R (2011). Study of filament wound grid-stiffened composite cylindrical structures. Compos. Struct. 93:1031-1038.
Han H, Cheng J, Taheri F, Pegg N (2006). Numerical and experimental investigations of the response of aluminum cylinder with a cutout subject to axial compression, Thin-Walled Struct. 44(2):254-270.
Kidane S, Li G, Helms J, Pang S, Woldesenbet E (2003). Buckling load analysis of grid stiffened composite cylinders. Compos. Part B 34:1-9.
Lekhnistskii G, Tsai WS, Cheron T (1968). Anisotropic plates. Gordon and Breach Science Publishers, New York.
Morozov EV, Lopatin AV, Nesterov VA (2011). Finite-element modeling and buckling analysis of anisogrid composite lattice cylindrical shells. Compos. Struct. 93:308-323.
Rahimi GH, Zandi M, Rasouli SF (2011). Analysis of the effect of stiffener profile on buckling strength in composite isogrid stiffened shell under axial loading. Aerospace Sci. Technol. pp. 1-6.
Ryu CH, Lee Y, Choi M, Kim Y (2004). Study on stress analysis of orthotropic composite cylindrical shells with a circular or an elliptical cutout. KSME Int. J. 18(5):808-813.
Vasiliev VV, Barynin VA, Rasin AF (2001). An isogrid lattice structures survey of development and application. Compos. Struct. 54:361-370.
Wodesenbet E, Kidane S, Pang S (2003). Optimization for buckling loads of grid stiffened composite panels. Compos. Struct. 60:159-169.
Yazdani S, Rahimi GH (2011). Stress analysis of grid cylindrical composite shells with circular cutout under axial compression. PPS 2011 Conference.
Yazdani M, Rahimi H, Khatibi AA, Hamzeh S (2009). An experimental investigation into the buckling of GFRP stiffened shells under axial loading. Sci. Res. Essays 9:914-920.
Yazdani M, Rahimi GH (2010). The effects of helical ribs' number and grid types on the buckling of thin-walled GFRP-stiffened shells under axial loading. Reinf. Plast. Compos. 29(17):2568-2575.
Yazdani M, Rahimi GH (2011). The behavior of GFRP-stiffened and – unstiffened shells under cyclic axial loading and unloading. Reinf. Plast. Compos. 30(5):440-445.